Seven-Year SSM/I-Derived Global Ocean Surface Turbulent Fluxes

Shu-Hsien Chou
Laboratory for Atmospheres
NASA Goddard Space Flight Center
Greenbelt, Maryland

Chung-Lin Shie
Science Systems & Applications, Inc.
Lanham, Maryland

Robert M. Atlas
Laboratory for Atmospheres
NASA Goddard Space Flight Center
Greenbelt, Maryland

Joe Ardizzone
General Sciences Corporation
Laurel, Maryland

Bulletin of the American Meteorological Society
June 2000

Corresponding author: Dr. Shu-Hsien Chou, Code 912, Laboratory for Atmospheres, NASA Goddard Space Flight Center, Greenbelt, MD 20771.
E-mail: chou@agnes.gsfc.nasa.gov

ABSTRACT

A 7.5-year (July 1987-December 1994) dataset of daily surface specific humidity and turbulent fluxes (momentum, latent heat, and sensible heat) over global oceans has been retrieved from the Special Sensor Microwave/Imager (SSM/I) data and other data. It has a spatial resolution of 2.0°x2.5° latitude-longitude. The retrieved surface specific humidity is generally accurate over global oceans as validated against the collocated radiosonde observations. The retrieved daily wind stresses and latent heat fluxes show useful accuracy as verified by those measured by the RV Moana Wave and IMET buoy in the western equatorial Pacific. The derived turbulent fluxes and input variables are also found to agree generally with the global distributions of annual- and seasonal-means of those based on 4-year (1990-93) comprehensive ocean-atmosphere data set (COADS) with adjustment in wind speeds and other climatological studies. The COADS has collected the most complete surface marine observations, mainly from merchant ships. However, ship measurements generally have poor accuracy, and variable spatial coverages. Significant differences between the retrieved and COADS-based are found in some areas of the tropical and southern extratropical oceans, reflecting the paucity of ship observations outside the northern extratropical oceans. Averaged over the global oceans, the retrieved wind stress is smaller but the latent heat flux is larger than those based on COADS. The former is suggested to be mainly due to overestimation of the adjusted ship-estimated wind speeds (depending on sea states), while the latter is suggested to be mainly due to overestimation of ship-measured dew point temperatures. The study suggests that the SSM/I-derived turbulent fluxes can be used for climate studies and coupled-model validations

1. Introduction

The global air-sea fluxes (momentum, latent and sensible heat, radiation, and freshwater) are the major forcing for driving oceanic circulation and, hence, are essential for understanding the general circulation of global oceans. These fluxes over the global oceans are required for driving ocean models and validating coupled ocean-atmosphere global models.

The project of comprehensive ocean-atmosphere data set (COADS) has collected the most complete surface marine observations since 1854, mainly from merchant ships (Woodruff et al. 1987). However, ship measurements generally have poor accuracy, variable spatial samplings, coarse temporal samplings, and fair-weather biases (Isemer and Hasse 1987; Kent et al. 1993; da Silva et al. 1994). It has generally been recognized that ships underestimate wind speeds at low to moderate winds ($< \sim 19$ m s^{-1}) but overestimate wind speeds at high winds (Kent and Taylor 1997). Da Silva et al. (1994) corrected biases for ship-estimated wind speeds and cloudiness, and then derived air-sea fluxes from the COADS and produced 1° x 1° latitude-longitude global monthly mean fluxes for the period 1945-93 (the results of 1990-93 are referred to as UWM/COADS in this study). Missing data, mostly in the tropical and southern oceans (south of 40°S), were filled through an objective analysis. There are other datasets of air-sea fluxes based on in situ measurements with adjustments in data or roughness lengths for flux computations (e. g., Isemer and Hasse 1987; Oberhuber 1988; Josey et al. 1999).

Satellite sensors can provide global coverages with adequate temporal samplings. Thus the development of satellite techniques for retrieving global air-sea fluxes is vital to climate studies. The latent heat flux at the ocean surface can be estimated from the sea surface temperature (SST), surface wind speed, and near surface specific humidity using an aerodynamic bulk method. Except for the surface humidity, these parameters can be directly retrieved from satellite radiance measurements. Thus the satellite retrieval of latent heat flux over oceans depends critically on the estimation of surface humidity. A number of techniques have been developed to retrieve surface humidity and latent heat fluxes from satellite observations (e. g., Chou et al. 1995, 1997, 2000;

Clayson and Curry 1996; Crewell et al. 1991; Curry et al. 1999; Esbensen et al. 1993; Liu 1986, 1988; Schlussel et al. 1995; Schulz et al. 1993, 1997; Wagner et al. 1990).

Chou et al. (1995) developed a method to retrieve instantaneous surface humidity from the radiances measured by the Special Sensor Microwave/Imager (SSM/I). Using both SSM/I-retrieved surface wind and humidity and other data, they then computed daily air-sea turbulent fluxes of momentum, latent and sensible heat over global oceans with a stability-dependent bulk scheme. Chou et al. (1997) improved the methods for retrieving the surface humidity (thus the latent heat flux) and sensible heat flux. Chou et al. (2000) further compared time series of SSM/I-retrieved daily turbulent fluxes with those of Improved Meteorological (IMET) buoy observed during the Tropical Ocean Global Atmosphere (TOGA) Coupled Ocean-Atmosphere Response Experiment (COARE) intensive observing period (IOP), from November 1992 to February 1993.

The SSM/I provides near-global coverage with improved coverage, spatial resolution, and accuracy over prior passive microwave instruments. It has been operating since July 1987 on a series of the Defense Meteorological Satellite Program (DMSP) spacecraft in a near-circular, sun-synchronous, and near-polar orbit with an orbit period of 102 minutes. The first (on F8 satellite) and second (on F10 satellite) SSM/Is provides data for the periods July 1987-December 1991, and January 1991-November 1997, respectively. The third (on F11 satellite), fourth (on F13 satellite), and fifth (on F14 satellite) SSM/Is has provided data since January 1992, May 1995, and May 1997, respectively. Thus since 1 January 1991, there have been at least two SSM/Is sensing the earth system with better spatial and temporal coverages. We have produced a 7.5-year (July 1987-December 1994) dataset of daily surface specific humidity and turbulent fluxes (momentum, latent heat, and sensible heat) over global oceans from the SSM/I data and other data, using the algorithm of Chou et al. (1997). It has a spatial resolution of 2.0°x2.5° latitude-longitude.

In this paper, we discuss the global distributions of 7-year (1988-94) annual and seasonal averages of the retrieved turbulent fluxes and input variables, as well as their retrieval accuracy. Section 2 describes the data sources used in this study. Section 3 briefly describes the

methodology and validation for the retrieval of surface humidity. To test the validity of the humidity-retrieval technique, instantaneous surface humidity retrieved from the F8 SSM/I during February and August 1988 and from the F10 and F11 SSM/Is during 1993 are compared with those collocated radiosonde observations over the global oceans. Section 4 briefly describes the methodology and validation for the retrieval of air-sea turbulent fluxes. To assess the retrieval accuracy, daily air-sea turbulent fluxes retrieved from the F10 and F11 SSM/Is are compared with those observed by the nearby RV Moana Wave during three separate cruises in the COARE IOP and by the IMET buoy during the entire COARE IOP. To check the accuracy of spatial and temporal variability of the retrieved fluxes, the global distributions of 1988-94 (and 1990-93) annual- and seasonal-mean turbulent fluxes and input variables, derived from the F8 and F11 SSM/Is, are compared with those of UWM/COADS (1990-93). The global distributions of 1988-94 annual- and seasonal-mean SSM/I fluxes and input variables are essential the same as those of 1990-93. The annual-mean results of both cases are compared with those of UWM/COADS in section 5. The former case (1988-94) emphasizes on the comparison of mean patterns, while the latter case is used to produce difference patterns for a quantitative comparison. The comparison of seasonal-means with those of UWM/COADS is given in section 6. The intercomparison can identify the strengths and weaknesses of the retrievals. It can also assess the quality of UWM/COADS, especially over the data-void regions of the tropical and southern oceans. Concluding remarks are given in section 7.

2. Data sources

The datasets used to derive surface humidity and air-sea turbulent fluxes are: 1) the SSM/I total precipitable water (entire column-integrated water vapor amount) and 10-m wind speeds of Wentz (1994), 2) the precipitable water in the lowest 500-m bottom-layer, 3) the 0Z and 12Z analyses of SST–T_{2m} (2-m temperatures) and sea-level pressures of the European Centre for Medium-Range Weather Forecasts (ECMWF), 4) the weekly mean SSTs of the National Centers for Environmental Prediction (NCEP), and 5) the SSM/I 10-m wind directions of Atlas (1996). The bottom-layer precipitable water is estimated from the SSM/I antenna temperatures of Wentz (1993)

using the method of Schulz et al. (1993). Daily mean SSTs for computing latent heat fluxes are interpolated from the weekly mean values of Reynolds and Smith (1994). The wind stress directions are taken from the SSM/I 10-m wind directions of Atlas et al. (1996), which used the 10-m wind speeds of Wentz (1994).

The SSM/I is a passive microwave radiometer, which senses the earth atmosphere system at four frequencies of 19.35, 22.235, 37.0 and 85.5 GHz. It has both horizontal and vertical polarization except for the 22 GHz water vapor channel that has only the vertical polarization measurement. Wentz (1994) developed his algorithm to retrieve simultaneously the 10-m wind speed, total precipitable water, columnar cloud water, and rain rate. These four geophysical parameters were derived by matching all the brightness temperatures of the five low frequency SSM/I channels to those computed using a radiative transfer model of the atmosphere and ocean. For a 25-km resolution, he found the root-mean-square (rms) differences to be 1.4 m s^{-1} for collocated SSM/I-buoy wind speeds, and 3.9 kg m^{-2} for collocated SSM/I-radiosonde total precipitable water. Since July 1987, the SSM/I has been operating on a series of DMSP satellites as mentioned in the introduction. In this study, the SSM/I data used for the collocation validation of surface humidity and turbulent fluxes are from the F8, F10, and F11 satellites, which have ascending equatorial crossings at 0612, 1942 and 1702 LT, respectively. The 1988-94 (and 1990-93) annual- and seasonal-mean turbulent fluxes and input variables are derived from the F8 and F11 SSM/Is, which have slightly better data quality compared to the F10 SSM/I (see section 3a).

To validate the estimated instantaneous surface humidity, twice-daily radiosonde observations at 30 stations over the global oceans (Table 1) for February and August 1988 and for 1993 are used to match the SSM/I retrievals. To validate the retrieved daily turbulent fluxes, the Moana Wave flux data (1.7°S, 156°E), and the latest version of the 7.5-min mean surface fluxes at the IMET buoy (1.75°S, 156°E) are used. The former were obtained from the COARE Surface Flux Summary - Release #2 (C. Fairall, private communication, 1994), while the latter were computed by Weller and Anderson (1996). To further assess the retrieval accuracy, the global distributions of 1990-1993

annual- and seasonal-mean turbulent fluxes and input variables of UWM/COADS (da Silva et al. 1994) are used.

3. Methodology and validation for retrieval of surface humidity

a. Methodology for retrieving surface humidity

Chou et al. (1995) developed a technique to retrieve instantaneous surface humidity from the SSM/I total precipitable water (W) and lowest 500-m bottom-layer precipitable water (W_B). The coefficients of surface-humidity retrieval equation (see Table 1 of Chou et al. 1997) were determined from the vertical profiles of the mean and first two empirical orthogonal functions (EOFs) of a sample population of humidity soundings of a given climatic regime. To retrieve surface humidity over global oceans, six sample populations and EOFs corresponding to six climate regimes were generated from 23177 FGGE IIb humidity soundings observed at 64 stations over global oceans during December 1978-November 1979 (Chou et al. 1995). The whole year's humidity soundings at these 64 stations were divided into 64 subsets of 6-month cold-season (November to April for the Northern Hemisphere and May to October for the Southern Hemisphere) and 64 subsets of 6-month warm-season humidity soundings. These 128 semiannual subsets were then grouped into six sample populations, according to their (subsets') semiannual-mean total precipitable water. The ranges of semiannual-mean total precipitable water of the six sample populations were set to be 0-10, 10-20, 20-30, 30-40, 40-50, and >50 kg m^{-2}, respectively, to group these 128 humidity subsets. The locations and mean total precipitable water of the subsets of the sample populations are highly related to the pattern and seasonal variation of the SST (see Figs. 1 and 2 of Chou et al. 1995). These six sample populations were thus considered as representing different climatic regimes for retrieving the surface humidity over global oceans.

Chou et al. (1995) found that the SSM/I-retrieved surface humidity agreed reasonably well with those of the radiosonde observations, COADS (Woodruff et al. 1987), and climatology estimated from ship measurements (Esbensen and Kushnir 1981). However, the derived surface humidity had a negative bias for the northern wintertime extratropical oceans but had a positive bias for the

northern summertime extratropical oceans, as compared to COADS. Chou et al. (1977) made two modifications to the original EOF method to improve the humidity biases. The negative humidity bias over the wintertime extratropical oceans ($W_B < 3$ kg m^{-2}) was mainly due to the underestimation of SSM/I W_B. Thus, they applied the surface humidity retrieved from the total precipitable water (more accurate than SSM/I W_B) as a lower limit for retrieving surface humidity in these dry regions. In this case, the coefficients of surface-humidity retrieval equation were determined from the vertical profiles of the mean and first EOF of humidity sample population of the corresponding climatic regime. On the other hand, the saturation specific humidity of daily SSTs was set to be the upper limits of retrieved surface humidity over the global oceans. This reduces the positive humidity bias over the summertime extratropical oceans. In the summer, as the warmer continental (or maritime) air moves over a colder ocean surface, fog or stratus may form with the surface air reaching saturation at a temperature near the underlying cold SST. Under this situation, the original method [as well as those of Liu (1986) and Schulz et al. (1993)] tends to overestimate the surface humidity. Chou et al. (1997) found that the global distributions and seasonal variability of the retrieved monthly surface humidity (and latent heat fluxes) were more realistic than those of Chou et al. (1995), as a result of these two modifications of humidity retrieval.

For the retrieval of the 7.5-year surface humidity, we use the total precipitable water of Wentz (1994). The bottom-layer precipitable water is estimated from the SSM/I antenna temperatures of Wentz (1993) using the method of Schulz et al. (1993). To retrieve the surface humidity, the previous mentioned W-ranges of the six sample populations are set to be the ranges for the observed W to select proper climatic regime and EOFs for the retrieval. The retrieval of surface humidity involves three steps: 1) to retrieve three values of surface humidity for the sample population corresponding to the observed SSM/I W and two neighboring sample populations (one drier and the other wetter), using the observed SSM/I W and W_B, 2) to compute a weighted mean from these three values of surface humidity, and 3) to limit the mean surface humidity with the saturation specific humidity of daily SST. The weights are derived from the probabilities that the observed SSM/I W is within the selected three sample populations. The probability is computed

using a normal distribution, with the mean and standard deviation taken from those of W of the selected sample population (Table 1 of Chou et al. 1995). The first humidity modification, using surface humidity retrieved from SSM/I W as lower bound, is restricted to the situations with the SSM/I W < 20 kg m^{-2} and the SSM/I W_B < 2.8 kg m^{-2} (mean W_B of the second driest sample population) for the wintertime extratropical oceans.

b. Collocation validation for retrieved surface humidity

To validate the retrieved instantaneous surface humidity, radiosonde observations at 30 stations over the global oceans (Table 1) are compared with the SSM/I retrievals within 100 km and 1.5 h. A single radiosonde observation can match several SSM/I cells (with a mean of ~50 for W and ~30 for W_B) within 100 km and 1.5 h. As these collocated SSM/I cells (with a single radiosonde observation) may not be independent samples, they are averaged and considered as a single sample for the collocation validation. Note that this approach is different from that of Schulz et al. (1997), who considered all the collocated SSM/I cells (with a smaller window) as independent samples to compute the retrieval errors. As the rms error decreases with increasing sample size, which depends on the collocation window, the retrieval accuracy presented by different studies should be compared with caution. Table 2 compares the retrieved surface humidity with those of radiosonde observations matched within 100 km and 1.5 h. Comparisons are carried out for three periods: February and August 1988, February and August 1993, and the entire annual cycle of 1993. Most radiosondes are launched at 0 and 1200 UTC. However, the ascending equatorial crossing times are 0612, 1942, and 1702 LT for the F8, F10 and F11 satellites, respectively. Thus, the collocated data pairs are 342 (F8) for February and August 1988, 462 (288 for F10 and 174 for F11) for February and August 1993, and 2054 (1205 for F10 and 849 for F11) for 1993.

As can be seen from Table 2, the retrieval of surface humidity is generally accurate over global oceans for the three periods tested during 1988 and 1993. The accuracy of surface humidity derived from the F8 and F11 SSM/Is is comparable and is slightly better than that derived from the F10 SSM/I. Table 2 shows that, for a 25-km spatial resolution, the surface humidity retrieved from

the F8 and F11 SSM/Is has small bias of 0.03-0.25 g kg^{-1}, rms difference of 1.55-1.62 g kg^{-1}, and a correlation coefficient of 0.97, as compared to the radiosonde observations over global oceans. The surface humidity retrieved from the F10 SSM/I reduces accuracy by 0.2-0.3 g kg^{-1} and SSM/I-radiosonde correlation by 0.03-0.04, as compared to the other two SSM/Is. The rms difference of surface humidity retrieved from the F8 SSM/I is smaller by 0.13 g kg^{-1}, as compared to that of Chou et al. (1995) for the same collocated data pairs during February and August 1988. This is due to the improvement in the retrieval of surface humidity mentioned above. Note that the humidity discrepancies between the SSM/Is and radiosondes may be due to the spatial and temporal mismatch as well as retrieval errors in surface humidity (and W and W_B) and errors in the radiosonde observations.

4. Methodology and validation for retrieval of air-sea turbulent fluxes

a. Methodology for retrieving air-sea turbulent fluxes

The turbulent fluxes are derived using a stability-dependent aerodynamic bulk scheme of Chou (1993), which was tested against aircraft covariance fluxes measured during cold air outbreaks off the middle Atlantic coast of the United States. This scheme is similar to Fairall et al. (1996) but without a gustiness parameterization, since it was found to have insignificant impact on the SSM/I turbulent fluxes (Chou et al. 1997). Using the surface-layer similarity theory, the turbulent fluxes are derived from the surface-layer scaling parameters by iteratively solving the diabatic profiles of wind, temperature, and moisture. The bulk transfer coefficients are stability dependent and are functions of wind speed, and sea-air temperature and humidity differences.

The turbulent fluxes are derived from daily mean values of SST, wind speed and specific humidity 10 m above the sea surface, and air temperature 2 m above the sea surface. It is noted that the reference height in the bulk scheme is set to 10 m for wind speed and humidity but is set to 2 m for temperature for correctly calculating their gradients and stability (Chou et al. 1997). The SSM/I 10-m wind speeds of Wentz (1994) are used, while the humidity retrieval is briefly discussed in the previous section. Wind stress directions are taken from the surface wind directions of Atlas et al.

(1996), which used the 10-m wind speeds of Wentz (1994) for input to a variational analysis. In this analysis, the wind speeds influence the directions assigned to them.

Daily mean SSTs used for computing latent heat fluxes are interpolated from the NCEP weekly mean SSTs, which have a spatial resolution of 1.0°x1.0° latitude-longitude (Reynolds and Smith 1994). To use an aerodynamic bulk scheme to derive surface sensible heat fluxes, the measurements of air temperatures in the atmospheric surface layer (about 50-100 m) are required. However, they are not currently available from satellite measurements. Thus, the $SST-T_{2m}$ used for computing the sensible heat flux is taken from the averages of 0Z and 12Z analyses of the ECMWF. Sea-air temperature difference is generally very small over the open ocean, except for the western Pacific warm pool and midlatitudes in the winter. Small errors in the SSTs and air temperatures could induce a relatively large error in the sea-air temperature difference if the errors are uncorrelated. The ECMWF analysis of 2-m temperatures is thermodynamically constrained to the SST.

b. Collocation validation for retrieved air-sea turbulent fluxes

Chou et al. (1997, 2000) have validated daily air-sea turbulent fluxes, derived from the F10 and F11 SSM/Is, with those measured at the nearby RV Moana Wave and IMET buoy during the COARE IOP, from November 1992 to February 1993. These results are summarized in Table 3. To compare with the SSM/I, Chou et al. (1997) derived daily mean turbulent fluxes at the RV Moana Wave from 1429 samples of 50-min mean air-sea turbulent fluxes from the COARE Surface Flux Summary - Release #2 (C. Fairall, private communication, 1994), which had a total sample of 1622. These 1429 selected samples covered 52 days. Of the 1429 samples of latent heat fluxes (wind stresses), 59% (77%) was the covariance fluxes, while 41% (23%) was the bulk fluxes computed by Fairall et al. (1996) using their bulk scheme. The covariance fluxes were used for samples with good data quality indicator, while the bulk fluxes were used for samples with poor quality indicator. Daily mean sensible heat fluxes at the RV Moana Wave were derived from the bulk fluxes computed by Fairall et al. (1996), as small sensible heat fluxes estimated using the eddy

correlation method may be sensitive to the measurement errors. Retrieved daily fluxes of the nearest grid box (2.0°x2.5° latitude-longitude) centered at (2°S, 155°E), were used for the comparison with the Moana Wave observations (1.7°S, 156°E).

For the comparison with the SSM/I, Chou et al. (2000) derived 120 days of daily mean turbulent fluxes at the IMET buoy from the latest version of the 7.5-min mean surface fluxes computed by Weller and Anderson (1996) using the bulk scheme of Fairall et al. (1996). The retrieved daily fluxes, interpolated to a 1.0°x1.0° latitude-longitude region centered at (1.5°S, 156°E), were used for the comparison with the IMET observations (1.75°S, 156°E). Table 3 shows that the retrieval accuracy of turbulent fluxes is comparable as validated with both the RV Moana Wave and IMET buoy. Daily wind stresses and latent heat fluxes (LHF) are retrieved with useful accuracy verified by both in situ measurements during the COARE IOP. The retrieved daily wind stresses have a bias of 0.0061 (-0.0018) N m^{-2}, an rms difference of 0.0187 (0.0211) N m^{-2}, and a correlation coefficient of 0.86 (0.78), as compared to the RV Moana Wave (IMET buoy). The retrieved daily latent heat fluxes have a bias of 6.2 (-2.4) W m^{-2}, an rms difference of 29.0 (29.2) W m^{-2}, and a correlation coefficient of 0.83 (0.71), as compared to the RV Moana Wave (IMET buoy). On the other hand, the retrieved daily sensible heat fluxes (SHF) are not in good agreement with those of the Moana Wave and IMET buoy. The poor quality of the retrievals is likely due to comparisons of small fluxes (having a mean of only ~6 W m^{-2}) with a large variability (associated with general weak winds and episodic events of strong westerly wind bursts and squalls). These results suggest that, with the assumption of independent daily errors, the rms errors to be 0.0042-0.0069 N m^{-2} for the retrieved monthly wind stress, 5.5-8.1 W m^{-2} for the retrieved monthly LHF, and 1.0-2.8 W m^{-2} for the retrieved monthly SHF.

Table 3 shows that the retrieved turbulent fluxes have small negative biases, as compared to the IMET buoy. Chou et al. (2000) found that this was mainly due to the fact that the retrievals underestimated the peak values of turbulent fluxes during westerly wind bursts and squalls, which were observed to accompany heavy rainfall (Anderson et al. 1996; Godfrey et al. 1998). Since winds associated with heavy rain events cannot be retrieved from the SSM/I data (Wentz 1994),

strong winds and, hence, peak turbulent fluxes are undersampled. The underestimation of the sensible heat flux may also caused by other factors, such as a smaller sea-air temperature difference of the ECMWF analysis and the exclusion of rainfall effect in the retrieval of sensible heat flux. The retrieval errors of the turbulent fluxes may also be due to spatial variability of the fluxes. The daily mean turbulent fluxes at the Moana Wave and IMET buoy were computed from the measurements covering small local areas. However, the retrieved daily fluxes used for the comparison with the Moana Wave (1.7°S, 156°E) were computed from the nearest low-resolution (2.0°x2.5° latitude-longitude) grid box centered at (2°S, 155°E). The retrieved daily fluxes of the nearest high-resolution (1.0°x1.0° latitude-longitude) grid box, centered at (1.5°S, 156°E), used for the comparison with the IMET buoy (1.75°S, 156°E) were interpolated from those of four low-resolution (2.0°x2.5° latitude-longitude) neighboring grid boxes. We anticipate that the turbulent fluxes computed on a high-resolution global grid of 1.0°x1.0° latitude-longitude will have better retrieval accuracy due to the improvement on resolution.

5. **Global distributions of annual-mean fluxes and input variables**

a. Comparison of 1988-94 annual mean with UWM/COADS

In this study, the results of UWM/COADS are interpolated to the same 2.0°x2.5° latitude-longitude global grid as that of the SSM/I for the comparisons. Figures 1-4 compare 7-year (1988-94) annual-mean turbulent fluxes and input variables, derived from F8 and F11 SSM/I data (Figs. 1 and 3), with those (1990-93) of UWM/COADS (Figs. 2 and 4). The SSM/I fluxes and input variables (Figs. 1 and 3) show large-scale coherent patterns, while those of UWM/COADS (Figs. 2 and 4) show small-scale eddy structures. The large-scale patterns of wind stresses (Figs. 1a and 2a) and wind speeds (Figs. 3a and 4a) are in general agreement between SSM/I and UWM/COADS. The maxima are located in the strong wind regions of trade winds and extratropical storm tracks. The minima are located in the weak wind areas of intertropical convergence zones (ITCZ), southern Pacific convergence zone (SPCZ), and subtropical highs.

However, the retrieved wind speeds (with a range of 5-10 m s^{-1}) and stresses (with a range of 0.25-1.5 N m^{-2}) are generally weaker and have smaller ranges than those of UWM/COADS.

The patterns of LHF (Figs.1b and 2b) and sea-air humidity difference, Q_S-Q (Figs. 3b and 4b), show some similarity between SSM/I and UWM/COADS. Large values of LHF are found in the Kuroshio Current and Gulf Stream areas resulting from high winds coupling with large Q_S-Q during cold air outbreaks in the winters. The LHF and Q_S-Q are maximized in the trade wind belts, and minimized in the high latitudes due to poleward decrease of the SST. The minimum LHF and Q_S-Q are also found in the eastern equatorial Pacific and Atlantic due to the up-welling induced cold SST associated with weak winds.

However, there are significant differences between these two flux datasets. The retrieved LHF in the trade wind regions (with the maxima of 180-200 W m^{-2}) are significantly larger than that of UWM/COADS. This is because the largest retrieved wind speed (~7-8 m s^{-1}) and Q_S-Q (~5-6 g kg^{-1}) are nearly collocated in the trade wind belts as they have coherent large-scale structures (Figs. 3a and 3b). On the other hand, the strongest winds (~9-11 m s^{-1}) and large Q_S-Q (~4-6 g kg^{-1}) of UWM/COADS are not collocated well in the trade wind belts as they have small-scale chaotic eddy structures (Figs. 4a and 4b). Furthermore, the maxima of Q_S-Q (up to 8 g kg^{-1}) of UWM/COADS are rather chaotic and are located in the western equatorial Pacific and the ITCZ in the eastern equatorial Pacific (near10°N, 120°W), which are associated with very weak winds and hence cannot produce large latent heat fluxes. The large values of Q_S-Q (up to 8 g kg^{-1}) in these regions, which are significantly larger than those (~5 g kg^{-1}) of SSM/I and Esbensen and Kushnir (1981), are likely to be overestimated as a result of the objective analysis in the undersampled areas of UWM/COADS. The SSM/I LHF and Q_S-Q are also significantly larger than those of UWM/COADS south of 40°S (See Fig 5b for the differences). The SHF (Figs. 1c and 2c) is generally very small due to the smallness of sea-air temperature difference (Figs. 3c and 4c), except for slightly larger fluxes in the northwestern parts of the North Pacific and North Atlantic caused by cold air outbreaks.

The global distributions of the fluxes and input variables of Esbensen and Kushnir (1981) are in better agreement with SSM/I (Figs. 1 and 3) than with UWM/COADS (Figs. 2 and 4), especially for the LHF and Q_S-Q. Compared to the climatologies of Esbensen and Kushnir (1981), the SSM/I wind speed is ~1 m s^{-1} higher in the tropics but is ~1 m s^{-1} lower in the extratropics; the Q_S-Q is 0.5-1 g kg^{-1} larger; and the LHF is ~20W m^{-2} larger in most of the oceans. The LHF differences are very small in the equatorial oceans but the SSM/I LHF is larger by ~40W m^{-2} in the southern trade wind belts. The SSM/I SHF is generally within ±5 W m^{-2} of Esbensen and Kushnir (1981).

b. 1990-93 annual difference with UWM/COADS

The period of 1990-93 is used for a quantitative comparison with the UWM/COADS. For the comparison, the SSM/I surface wind speeds (U_{20m}), specific humidity (Q_{20m}), and temperature (T_{20m}) are adjusted to the 20-m level (same as that of UWM/COADS) using the aerodynamic bulk scheme of the flux derivation. The SSM/I-minus-UWM/COADS differences of annual-mean fluxes and input variables for 1990-93 are shown in Figs. 5 and 6. Figure 5a and 6a show that the retrieved wind stress and U_{20m} are generally smaller than those of UWM/COADS, with significant differences (~0.05-0.1 N m^{-2} and ~2-3 m s^{-1}) over the high wind regions of northern extratropics and trade winds. In the central equatorial Pacific and southern extratropical oceans, wind speeds and wind stresses show significant positive and negative differences between SSM/I and UWM/COADS, likely a result of the objective analysis to fill undersampled areas of the latter (further discussed later).

Further comparison with the global distribution of 1970-89 annual-mean ship-measured 20-m winds of da Silva et al. (1994) indicates that the 1990-93 annual-mean SSM/I 20-m wind speeds (not shown, about 6% higher than that of Fig. 3a) are fairly accurate. This comparison reveals a good agreement in the tropics, with the SSM/I wind speeds lower by ~1 m s^{-1} in the extratropical North Atlantic and southern extratropics, and lower by 1-2 m s^{-1} in the extratropical North Pacific. This discrepancy is likely partly due to higher heights of the actual ship anemometers and partly

due to interannual variability. Da Silva et al. (1994) applied an anemometer height of 20 m to the entire anemometer-measured wind dataset of voluntary observing ships for correcting the ship-estimated wind speeds (depending on sea states). The assumed 20-m anemometer height is significantly lower than the actual heights, especially over the northern extratropical oceans during late 80's and beyond (Kent and Taylor 1997). Thus the negative differences of wind speeds and stresses shown in Figs 5a and 6a are likely mainly due to the overestimation from UWM/COADS, as the SSM/I wind speeds were tuned to 38000 buoy winds with high degree of accuracy (Wentz 1994).

Figure 5b shows that the SSM/I LHF is generally larger than that of UWM/COADS, but is slightly smaller in the weak wind areas (ITCZs, SPCZ, and subtropics). The discrepancy of LHF between the two flux datasets follows closely that of Q_S-Q_{20m} but not that of wind speed (Figs. 5b, 6a, and 6b). This is because significant discrepancy of Q_S-Q_{20m} is generally associated with high winds to enhance humidity effect, while significant discrepancy of wind speed is generally associated with small Q_S-Q_{20m} to reduce the impact of wind speed. In the equatorial Pacific and Southern Hemispheric oceans, Figs. 5b, 6a and 6b show some adjacent areas of large positive and negative differences of LHF, wind speed, and Q_S-Q_{20m}. Data are generally missing or undersampled in these areas (da Silva et al. 1994; Chou et al 1997; Wolter 1997). These positive and negative differences are mainly due to shifts in the positions of the maxima or minima of these variables between SSM/I and UWM/COADS (see Figs. 1-4). The former has large-scale smooth patterns, while the latter has small-scale chaotic patterns with extreme values located generally in these areas. Thus, the large differences likely result from the objective analysis in the undersampled areas of the latter. Figure 6c shows that the discrepancy of SST-T_{20m} between the two flux datasets is generally small, except for some undersampled areas mentioned above. Thus, the SSM/I SHF is generally within ± 10 W m^{-2} of UWM/COADS, except for undersampled areas and some small areas in the extratropics, which are mainly due to the difference in wind speeds (Figs. 5c, 6a, and 6c).

Figure 7 shows 4-year (1990-93) annual-mean 20-m specific humidity for the SSM/I, UWM/COADS, and their difference (UWM/COADS-minus-SSM/I). Figures 7a and 7b show that the maximum humidity is located in the equatorial Indian Ocean, western Pacific warm pool and ITCZs, where the SST has maximum. The minimum humidity is located in the Polar Regions as the SST decreases poleward. The SSM/I humidity (Fig. 7a) shows the large-scale coherent pattern closely following that of the SST, including the cold tongues in the eastern South Pacific and South Atlantic. On the other hand, the specific humidity of UWM/COADS (Fig. 7b) in the Southern Hemisphere undulates in the zonal direction and does not follow the SST pattern. Figure 7c shows that the retrieved surface humidity is wetter in the weak wind areas (ITCZs, SPCZ, and subtropics) but is drier in the high wind regions (trade winds, extratropics) than that of UWM/COADS, with the difference in some undersampled areas exceeding ± 2 g kg^{-1}. Comparing Figs. 6b and 7c, we can see that the discrepancy field of Q_S-Q_{20m} between the two flux datasets (Fig. 6b) follows closely that of surface humidity (Fig. 7c), as the effect of SST difference is either very small or outweighed by that of humidity differences.

To investigate regional discrepancies of surface humidity between SSM/I and UWM/COADS, we have compared the SSM/I (F11) retrieved surface humidity with those of radiosonde observations within 100 km and 1.5 h for various regions during 1993. For four regions of tropical Indian Ocean (20°S-20°N, 70°E-110°E), Caribbean sea (10°N-25°N, 90°W-50°W), southern extratropical Indian Ocean (35°S-45°S, 70°E-80°E), and southern extratropical Pacific Ocean (50°S-60°S, 150°E-180°E), the SSM/I surface humidity has biases of 0.51, -0.11, -0.13, and -0.10 g kg^{-1}, respectively, as compared to the radiosonde observations. However, Fig. 7c shows that the surface humidity of UWM/COADS at the radiosonde stations of these four regions (see Table 1) is generally higher than that of SSM/I by >1 g kg^{-1}. This result is consistent with some previous findings that ships overestimated dew point temperatures (by ~0.5°C), which resulted a higher value of surface humidity for COADS (Isemer and Hasse 1987; Kent et al. 1993; da Silva et al. 1994). Chou et al. (1997) also found that the radiosonde observed surface humidity of February and

August 1993 was more close to that of SSM/I than that of COADS. Thus, the results suggest that the global distribution of surface humidity is more realistic for SSM/I (Fig. 7a).

Table 4 summarizes the area-averages of SSM/I-minus-UWM/COADS difference of 1990-93 annual-mean fluxes and input variables for various latitude belts of the global oceans. It can be seen that the area-mean differences of Q_{20m} for various latitude belts dominate that of Q_S-Q_{20m}, as the average differences of SST are very small. The differences averaged over the global oceans are -0.0166 N m^{-2} for wind stress, 18.54 W m^{-2} for LHF, -0.81 W m^{-2} for SHF, -0.48 m s^{-1} for U_{20m}, -0.56 g kg^{-1} for Q_{20m}, 0.52 g kg^{-1} for Q_S-Q_{20m}, 0.27°C for SST-T_{20m}, and 0.16°C for SST. These results differ insignificantly from those averaged over 60°S-60°N. The area-mean wind stresses and speeds of SSM/I for all the latitude belts are significantly smaller than those of UWM/COADS, especially over the northern extratropical oceans (with differences of -0.0532 N m^{-2} and -1.46 m s^{-1}). The small average differences of wind stress and speed in the southern extratropical oceans are because of cancellation of large positive and negative deviations (Figs. 5a and 6a). The retrieved area-mean LHF and Q_S-Q_{20m} are larger than those of UWM/COADS by 11.77-13.20 W m^{-2} and 0.42-0.54 g kg^{-1} in the tropical and northern extratropical oceans, but are significantly larger in the southern extratropical oceans (with differences of 31.41 W m^{-2} and 0.70 g kg^{-1}). The retrieved area-mean SHF is slightly smaller in the tropical oceans, but is significantly smaller in the northern extratropical ocean (with a difference of -5.49 W m^{-2}), as the SSM/I wind speed is significantly smaller than that of UWM/COADS there.

Some climatological studies suggested that the latent heat fluxes based on ship measurements might be systematically underestimated (Bunker et al. 1982; Oberhuber 1988; da Silva et al. 1994; Josey et al. 1998). Bunker et al. (1982) found that latent heat fluxes determined from ship measurements (with a large moisture transfer coefficient of about 1.4×10^{-3}) were underestimated by 29 W m^{-2} and 48 W m^{-2} for the Mediterranean and Red Seas, respectively, based on the heat balance of both seas. Using the COADS original dew point temperatures with revised wind speeds, da Silva et al. (1994) found that the long-term (1945-89) annual-mean net heat flux into the ocean

was 30.2 W m^{-2} over the entire ocean. They thought that the surplus of heat flux was mainly due to the overestimation of solar radiation and the underestimation of latent heat flux. To achieve a global heat balance, they constrained the heat fluxes by the meridional oceanic heat transport and found that the solar radiation needed to reduce by 7% and the latent heat flux needed to increase by 15-17%. This result is consistent with Table 4 that the retrieved LHF averaged over the entire ocean is larger than that of UWM/COADS by 18.54 W m^{-2}, which is 20% of the latter (unconstrained LHF used in this study). Josey et al. (1998) found similar imbalance for their COADS-based air-sea flux estimates. Oberhuber (1988) also constrained his COADS-derived surface Fluxes by reducing solar radiation (10%) and increasing latent heat flux (using the enhanced roughness length to increase the transfer coefficient). Thus, the retrieved LHF is likely to be accurate. The LHF difference between both datasets is likely mainly due to the humidity overestimation of UWM/COADS (with some cancellations of random errors due to the objective analysis in the undersampled areas), although the SSM/I surface humidity and wind speed are subject to retrieval errors.

6. Global distributions of seasonal-mean fluxes and input variables

In this section, we focus on the seasonal variations of wind stress, 10-m wind speed, latent heat flux, and sea-air humidity difference for the winter (December, January, and February), spring (March, April, and May), summer (June, July, and August), and fall (September, October, and November) of 1988-94. Figures 8 and 9 show 7-year (1988-94) seasonal-mean wind stresses and 10-m wind speeds, derived from F8 and F11 SSM/I data, respectively. The maximum wind stresses and speeds are generally found in the trade wind zones, the tropical Indian ocean (associated with the southwest summer Monsoon circulation), the wintertime extratropical North Pacific and North Atlantic oceans (associated with synoptic activities), and the extratropics of the Southern Hemisphere. Wind speeds and stresses of the trade wind zones are generally larger in the Northern Hemisphere than in the Southern Hemisphere during the winter and spring, and vise versa during the other two seasons as a result of seasonal variations of the Hadley circulations.

The minimum wind stresses and speeds are generally found in the tropical Indian ocean and SPCZ during the winter and spring, near Indochina during the summer and fall, in the eastern Pacific and Atlantic Oceans associated with the seasonally marched ITCZs, and the seasonally matched subtropical highs in both hemispheres. The retrieved wind and stress fields clearly show the seasonal variation of the atmospheric general circulation and are consistent with those of Atlas et al. (1996), Esbensen et al. (1993), Chou et al. (1995), and Hellerman and Rosenstein (1983). The large-scale patterns and seasonal variations of wind stresses and wind speeds are similar between SSM/I (1988-94, and 1990-93) and those (1990-93) of UWM/COADS (not shown). However, the retrieved seasonal-mean wind stresses and 20-m wind speeds are generally smaller than those of UWM/COADS, with the 1990-93 seasonal differences (not shown) similar to those of the annual differences (Figs. 5a and 6a) but with seasonal variations mainly in the northern extratropics.

Figures 10 and 11 show 7-year (1988-94) seasonal-mean LHF and sea-air (10 m) humidity differences, Q_S-Q_{10m}, derived from F8 and F11 SSM/I data, respectively. It can be seen that the seasonal variability of LHF follows essentially that of Q_S-Q_{10m} and that both are larger in the winter than in the summer hemisphere, as a result of seasonal variation of the atmospheric general circulation. The maxima of LHF (160-240 W m^{-2}) are generally found in the trade wind zones of both hemispheres, resulting from larger Q_S-Q_{10m} coupled with stronger winds (5-7 g kg^{-1}, and 7-10 m s^{-1}). In the trade wind zones, the largest values of wind speed, Q_S-Q_{10m}, and LHF are in the winter hemisphere due to the strongest wintertime Hadley circulations (see Figs 9-11). Near the Kuroshio Current and Gulf Stream areas, the LHF is maximized in the winter with the magnitudes of ~240-280 W m^{-2} (Fig. 10a). This is because of a large increase in the wintertime wind speed and Q_S-Q_{10m} (Figs. 9a and 11a), due to cold air outbreaks over warm oceans (e.g., Agee and Howley 1977; Chou and Ferguson 1991; Chou 1993). The LHF and Q_S-Q_{10m} decrease poleward as the SST decreases poleward, with the minima in the high latitudes of the summer hemisphere. The minima of LHF and Q_S-Q_{10m}, associated with weak winds, are also found in the eastern equatorial Pacific and Atlantic for all seasons due to the up-welling induced cold SST. The large-scale

patterns and seasonal variations of LHF and Q_S-Q_{10m} for the winter and summer are consistent with those (February and August 1993) of Chou et al. (1997).

The patterns of the retrieved seasonal-mean LHF and Q_S-Q_{10m} are somewhat different from those of UWM/COADS (not shown). The latter has very small seasonal variability for Q_S-Q_{20m}, with the seasonal-mean fields generally close to that of the annual-mean (Fig.4b). The latter also has relatively small seasonal variability for LHF, except for the northern extratropics mainly due to the seasonal variability of wind speeds. The patterns of seasonal differences (SSM/I-minus-UWM/COADS) of LHF and Q_S-Q_{20m} (not shown) are similar to those (February and August 1993) of Chou et al. (1997) over the regions without missing data of COADS. These patterns have the same characteristic as that of their annual differences (Figs. 5b and 6b) but with some seasonal variations,

The1990-93 seasonal variations (winter-minus-summer) of LHF, Q_S-Q_{20m}, and U_{20m} for various regions are shown in Table 5. The seasonal variations of LHF for SSM/I (UWM/COADS) are 88.16 (59.55), 39.18 (23.18), -37.19 (-24.11), and -30.76 (-11.79) W m^{-2} for the oceans in the regions of 30°N-60°N, 0-30°N, 0-30°S, and 30°S-60°S, respectively. The seasonal variations of Q_S-Q_{20m} for SSM/I (UWM/COADS) are 1.72 (0.79), 0.61 (0.26), -0.60 (-0.13), and -0.53 (-0.01) g kg^{-1} for the oceans in the regions of 30°N-60°N, 0-30°N, 0-30°S, and 30°S-60°S, respectively. The results show that the LHF, Q_S-Q_{20m}, and U_{20m} are larger in the winter than in the summer of each hemisphere (for both SSM/I and UWM/COADS), as a result of seasonal variation of the atmospheric general circulation. However, the seasonal variability of the retrieved LHF and Q_S-Q_{20m} is larger than that of UWM/COADS (especially in the southern extratropics), although the seasonal variability of wind speeds is comparable. The small seasonal variability for UWM/COADS reflects the paucity of ship observations outside the northern extratropics.

7. Concluding remarks

A 7.5-year (July 1987-December 1994) dataset of daily surface humidity and turbulent fluxes over global oceans has been produced from the SSM/I data and other data, using the algorithm of

Chou et al. (1997). It has a spatial resolution of 2.0°x2.5° latitude-longitude. The retrieved surface humidity is generally accurate over global oceans, for the tested period of February and August 1988 and the entire annual cycle of 1993, as validated against the collocated radiosonde observations. The retrieved daily wind stresses and latent heat fluxes show useful accuracy as verified by those of the RV Moana Wave and IMET buoy measured during the COARE IOP.

The global distributions of 1988-94 (and 1990-93) annual- and seasonal-mean turbulent fluxes and input variables, derived from the F8 and F11 SSM/Is, agree generally with those of UWM/COADS (1990-93) of da Silva et al. (1994) and other climatological studies. However, there are significant differences between SSM/I and UWM/COADS, especially in the undersampled areas of the latter. The retrieved turbulent fluxes and input variables show large-scale coherent patterns, while those of UWM/COADS show small-scale eddy structures, especially in the equatorial Pacific and southern extratropical oceans. The retrieved wind stress and speed are systematically smaller than those of UWM/COADS over the high wind regions of northern extratropics and trade winds. This discrepancy is suggested to be mainly due to underestimation of the ship anemometer's heights by da Silva et al. (1994), especially over the northern extratropical oceans (Kent and Taylor 1997). Wind speeds at the heights equivalent to that of the anemometers can be estimated from the sea states based on the measurements from the anemometers. If the heights of anemometers are underestimated, the higher wind speeds measured at high levels are assigned to the low levels. This can cause the measured and estimated wind speeds to be too high.

The retrieved surface humidity in general shows realistic large-scale coherent patterns closely following that of the SST including the cold tongues in the eastern South Pacific and South Atlantic. On the other hand, the surface humidity of UWM/COADS in the Southern Hemisphere undulates in the zonal direction and does not follow the SST patterns. The retrieved surface humidity is generally drier than that of UWM/COADS in the high wind regions of trade winds and extratropics and compares better with radiosonde observations. This result is consistent with some previous findings that ships overestimated dew point temperatures (Isemer and Hasse 1987; Kent et al. 1993; da Silva et al. 1994; Chou et al. 1997). The retrieved latent heat flux and sea-air humidity

difference also show more realistic large-scale coherent patterns with larger seasonal variability, especially over the tropics and southern extratropical oceans. This reflects the paucity of ship observations outside the northern extratropical oceans. Averaged over the global oceans, the retrieved 1990-93 annual-mean latent heat flux and Q_S-Q_{20m} are larger than those of UWM/COADS by 18.54 W m^{-2} and 0.52 g kg^{-1}, respectively. This result is consistent with previous studies that the latent heat fluxes based on ship measurements might be systematically underestimated (Bunker et al. 1982; Oberhuber 1988; da Silva et al. 1994; Chou et al. 1997; Josey et al. 1998).

The results suggest that the SSM/I-derived turbulent fluxes can be used for climate studies and coupled-model validations. Current work is aimed at producing a high-resolution (1° x 1° latitude-longitude) dataset of daily global ocean surface turbulent fluxes. We plan to use the Pathfinder 10-m wind speeds and total precipitable water of Wentz (1995). This flux dataset is anticipated to have a better retrieval accuracy due to improved data and resolution.

Acknowledgments This study was supported by the TRMM Program and Physical Oceanography Program, NASA/Office of Earth Science. The SSM/I data of total precipitable water, wind speeds, and antenna temperatures were provided by F. Wentz. The NCEP SSTs were provided by R. W. Reynolds. The sea-air temperature differences were provided by the ECMWF. The flux data of the RV Moana Wave were provided by C. Fairall. The 7.5-min mean turbulent fluxes of IMET buoy were computed by R. A. Weller and S. P. Anderson. The COADS turbulent fluxes were provided by A. da Silva. Consultation related to the computer codes of the Wentz SSM/I brightness temperature was provided by G. J. Huffman and P. R. Keehn.

REFERENCES

Agee, E. M. and R. P. Howley, 1977: Latent and sensible heat flux calculations at the air-sea interface during AMTEX 74. *J. Appl. Meteor., **16,*** 443-447.

Anderson, S. P., R. A. Weller, and R. B. Lukas, 1966: Surface buoyancy forcing and the mixed layer of the western Pacific warm pool: observations and 1D model results. *J. Climate,* **9**, 3056-3085.

Atlas, R., R. N. Hoffman, S. C. Bloom, J. C. Jusem, and J. Ardizzone, 1996: A Multiyear Global Surface Wind Velocity Dataset Using SSM/I Wind Observations. *Bull. Amer. Meteor. Soc.*, **77**, 869-882.

Bunker, A. F., H. Charnock and R.A. Goldsmith, 1982: A note on the heat balance of the Mediterranean and Red Seas. *J. Mar. Res.*, **40**, 73-84.

Chou, S.-H., 1993: A comparison of airborne eddy correlation and bulk aerodynamic methods for ocean-air turbulent fluxes during cold-air outbreaks. *Bound.-Layer Meteor.*, **64**, 75-100.

Chou, S.-H. and M. P. Ferguson, 1991: Heat Fluxes and Roll Circulations over the Western Gulf Stream During an Intense Cold-Air Outbreak. *Bound.-Layer Meteor.*, **55**, 255-281.

Chou, S.-H., R. M. Atlas, C.-L. Shie and J. Ardizzone, 1995: Estimates of surface humidity and latent heat fluxes over oceans from SSM/I data. *Mon. Wea. Rev.*, **123**, 2405-2425.

Chou, S.-H., C.-L. Shie, R. M. Atlas and J. Ardizzone, 1997: Air-sea fluxes retrieve from Special Sensor Microwave Imager data. *J. Geophys. Res.*, **102**, 12705-12726.

Chou, S.-H., W. Zhao, and M.-D. Chou, 2000: Surface heat budgets and sea surface temperature in the Pacific warm pool during TOGA COARE. *J. Climate,* **13**, 634-649.

Clayson, C. A. and J. A. Curry, 1996: Determination of surface turbulent fluxes for the Tropical Ocean-Global Atmosphere Coupled Ocean-Atmosphere Response Experiment: Comparison of satellite retrievals and in situ measurements. *J. Geophys. Res.*, **101**, 28515-28528.

Crewell, S., E. Ruprecht and C. Simmer, 1991: Latent heat flux over north Atlantic ocean-a case study. *J. Appl. Meteor., **30,*** 1627-1635.

Curry, J. A., C. A. Clayson, W. B. Rossow, R. Reeder, Y.-C. Zhang, P. J. Webster, G. Liu, R.-S. Sheu, 1999: High-resolution satellite-derived dataset of the surface fluxes of heat, freshwater, and momentum for the TOGA COARE IOP. *Bull. Amer. Meteor. Soc.*, **80**, 2059-2080.

da Silva, A, C. C. Young and S. Levitus, 1994: Atlas of Surface Marine Data 1994 Vol. 1: Algorithms and Procedures. NOAA Atlas NESDIS 6, US Dept. of Commerce, NOAA, NESDIS, Washington, DC, 83 pp.

Esbensen S. K. and Y. Kushnir, 1981: The heat budget of the global ocean: An atlas based on estimates from surface marine observations. Rep. 29, Climatic Research Institute, Oregon State University, Corvallis, Oregon, 27pp.

Esbensen, S. K., D. B. Chelton, D. Vickers and J. Sun, 1993: An analysis of errors in Special Sensor Microwave Imager evaporation estimates over the global oceans. *J. Geophys. Res., 98 (C4),* 7081-7101.

Fairall, C., E. F. Bradley, D. P. Rogers, J. B. Edson, and G. S. Young, 1996: Bulk parameterization of air-sea fluxes for Tropical Ocean Global Atmosphere Coupled Ocean-Atmosphere Response Experiment. *J. Geophys. Res.*, **101** (C2), 3747-3764.

Godfrey, J. S., R. A. House Jr., R. H. Johnson, R. Lukas, J.-l. Redelsperger, A. Sumi, and R. Weller, 1998: Coupled Ocean-Atmosphere Response Experiment (COARE): An interim report. *J. Geophys. Res.*, **103**, 14395-14450.

Hellerman , S. and M. Rosenstein, 1983: Normal monthly wind stress over the world ocean with error estimates. *J. Phys. Oceanogr.,* **13**, 1093-1104.

Isemer, H.-J. and L. Hasse, 1987: The Bunker Atlas of the North Atlantic Ocean. Vol. 2: Air-sea interactions. Springer Verlag, 252 pp.

Josey, S. A., E. C. Kent and P. K. Taylor 1999: New insights into the ocean heat budget closure problem from analysis of the SOC air-sea flux climatology. *J. Climate*, **12**, 2856 - 2880.

Kent, E. C., P. K. Tayor, B. S. Truscott and J. S. Hopkins, 1993: The accuracy of voluntary observing ship's meteorological observations - Results of the VSOP-NA. *J. Atmos. & Oceanic Tech., 10,* 591-608.

Kent, E. C., and P. K. Taylor, 1997: Choice of a Beaufort equivalent scale. *J. Atmos. Oceanic Technol.*, **14**, 228-242.

Liu, W. T., 1986: Statistical relation between monthly precipitable water and surface-level humidity over global oceans. *Mon. Wea. Rev.*, **114**, 1591-1602.

Liu, W. T., 1988: Moisture and latent heat flux variabilities in the tropical Pacific derived from satellite data. *J. Geophys. Res., 93,* 6749-6760+ plates on 6965-6968.

Oberhuber, J. M., 1988: *An Atlas Based on the COADS Data Set: The Budgets of Heat, Buoyancy, and Turbulence Kinetic Energy at the Surface of the Global Ocean.* Rep. No. 15, Max-Plank Inst. for Meteorol., Hamburg, Germany.

Reynolds, R. W. and T. S. Smith, 1994: Improved global sea surface temperature analyses. *J. Climate.*, **7**, 929-948.

Schluessel, P., L. Schanz, and G. Englisch, 1995: Retrieval of latent heat flux and longwave irradiance at the sea surface from SSM/I and AVHRR measurements. *Adv. Space Res.*, **16**, 107-116.

Schulz, J., P. Schluessel and H. Grassl, 1993: Water vapor in the atmospheric boundary layer over oceans from SSM/I measurements. *Int. J. Rem. Sens.*, **14**, 2773-2789.

Schulz, J., J. Meywerk, S. Ewald, and P. Schluessel, 1997: Evaluation of satellite-derived latent heat fluxes. *J. Climate*, **10**, 2782-2795.

Wagner, D., E. Ruprecht and C. Simmer, 1990: A combination of microwave observations from satellites and EOF analysis to retrieve vertical humidity profiles over the ocean. *J. Appl. Meteor., 29,* 1142-1157.

Weller R. A. and S. P. Anderson, 1996: Surface meteorology and air-sea fluxes in the western equatorial Pacific warm pool during the TOGA Coupled Ocean-Atmosphere Response Experiment. *J. Climate,* **9**, 1959-1990.

Wentz, F. J., 1993: User's Manual SSM/I Antenna Temperature Tapes. Revision 2. Tech. Rep. 060989, 16 pp. [Available from Remote Sensing Systems, Santa Rosa, CA 95404.]

Wentz, F. J., 1994: User's Manual SSM/I-2 Geophysical Tapes. Tech. Rep. 070194, 20 pp. [Available from Remote Sensing Systems, Santa Rosa, CA 95404.]

Wentz, F. J., 1995: A well calibrated ocean algorithm for SSM/I. Tech. Rep. 070195, 34 pp. [Available from Remote Sensing Systems, Santa Rosa, CA 95404, http://www.ssmi.com].

Wolter, K., 1997: Trimming problems and remedies in COADS. *J. Climate.*, **10**, 1980-1997.

Woodruff, S. D., R. J. Slutz, R. L., Jenne and P. M. Steurer, 1987: A comprehensive ocean-atmosphere data set. *Bull. Amer. Meteor. Soc.*, **68**, 1239-1250.

Table 1. Radiosonde stations for collocation validation.

Name	Number	Latitude	Longitude
	Indian Ocean		
Port Blair	43333	11.67°N	92.72°E
Minicoy Island	43369	8.30°N	73.00°E
Seychelles	63985	4.67°S	55.52°E
Diego Garcia	61967	7.35°S	72.48°E
Cocos Island	96996	12.18°S	96.83°E
I. N. Amsterdam	61996	37.80°S	77.53°E
	Pacific Ocean		
St. Paul Island	70308	57.15°N	170.22°W
Nikolskoye-on-Bering	32618	55.20°N	165.98°E
Hachijajima	47678	33.12°N	139.78°E
Minamidaito	47945	25.83°N	131.23°E
Ishigakijima	47918	24.33°N	124.17°E
Isla Guadalupe	76151	29.17°N	118.32°W
Isla Socorro	76723	18.72°N	110.95°W
Wake Island	91245	19.28°N	166.65°E
Guam	91217	13.55°N	144.83°E
Willis Island	94299	16.30°S	149.98°E
Pago Pago	91765	14.33°S	170.72°W
Tahiti Island Faaa	91938	17.55°S	149.62°W
Easter	85469	27.17°S	109.43°W
Lord Howe Island	94995	31.53°S	159.08°E
Campbell Island	93944	52.55°S	169.15°E
Macquarie Island	94998	54.50°S	158.95°E
	Atlantic Ocean		
Mike	C7M	66.00°N	2.00°E
Lima	C7L	57.00°N	20.00°W
Sable Island	71600	43.93°N	60.02°W
Bermuda NAS/Kindley	78016	32.37°N	64.68°W
Roberts Field	78384	19.30°N	81.37°W
San Maarten	78866	18.05°N	63.12°W
Barbados	78954	13.07°N	59.50°W
Isla San Andreas	80001	12.58°N	81.70°W

Table 2. Comparison of retrieved surface humidity with those of radiosonde observations within 100 km and 1.5 h. In the table mean denotes retrieved mean humidity for N collocated data during the periods indicated, positive bias indicates larger retrieved values, and rms denotes the root-mean-square difference. Units are g kg^{-1}.

Satellite	Period	N	Mean	Bias	Rms	Correlation
F8	Feb/88, Aug/88	342	11.61	0.03	1.57	0.97
F10	Feb/93, Aug/93	288	8.95	0.00	1.78	0.94
F11	Feb/93, Aug/93	174	11.35	0.10	1.55	0.97
F10	1993	1205	8.73	0.14	1.96	0.93
F11	1993	849	11.96	0.25	1.62	0.97

Table 3. Comparison of daily wind stresses, latent heat fluxes (LHF), and sensible heat fluxes (SHF) derived from the F10 and F11 SSM/Is with those measured at the RV Moana Wave (MW) and IMET buoy during COARE IOP. In the table mean denotes retrieved fluxes averaged over 52 (120) days for the MW (IMET), positive bias indicates larger retrieved fluxes, and rms denotes the root-mean-square difference. Units are W m^{-2} for heat fluxes and 10^{-4} N m^{-2} for wind stress.

Data source	Number of days	Flux	Mean	Bias	Rms		Correlation
					Daily	Monthly	
MW	52	stress	417	61	187	69	0.86
IMET	120	stress	371	-18	211	42	0.78
MW	52	LHF	110.7	6.2	29.0	8.1	0.83
IMET	120	LHF	104.8	-2.4	29.2	5.5	0.71
MW	52	SHF	5.8	0.8	3.8	1.0	0.39
IMET	120	SHF	6.3	-2.6	6.6	2.8	0.40

Table 4. Differences (SSM/I-minus-UWM/COADS) of annual-mean (1990-93) wind stress, latent heat flux (LHF), sensible heat flux (SHF) and input variables for various regions of the global oceans. In the table, U_{20m}, Q_{20m}, and T_{20m}, are the wind speed, specific humidity, and temperature at the 20 m height, while Q_S is the sea level specific humidity.

Variables	Units	90°S-90°N	60°S-60°N	30°S-30°N	30°N-60°N	30°S-60°S
Stress	$N\ m^{-2}$	-0.0166	-0.0184	-0.0187	-0.0532	0.0011
LHF	$W\ m^{-2}$	18.54	17.25	11.77	13.20	31.41
SHF	$W\ m^{-2}$	-0.81	-1.10	-0.64	-5.49	-0.20
U_{20m}	$m\ s^{-1}$	-0.48	-0.71	-0.68	-1.46	-0.33
Q_{20m}	$g\ kg^{-1}$	-0.56	-0.51	-0.32	-0.54	-0.91
$Q_S - Q_{20m}$	$g\ kg^{-1}$	0.52	0.51	0.42	0.54	0.70
$SST - T_{20m}$	°C	0.27	0.30	0.28	0.37	0.28
SST	°C	0.16	-0.05	0.06	-0.09	-0.29

Table 5. Comparison of 1990-93 seasonal variations (DJF-JJA) of latent heat flux (LHF), sea-air humidity difference ($Q_S - Q_{20m}$), and 20-m wind speed (U_{20m}) for various regions of the global oceans between SSM/I and UWM/COADS.

Variables	Units	Source	30°N-60°N	0-30°N	0-30°S	30°S-60°S
LHF	$W\ m^{-2}$	SSM/I	88.16	39.18	-37.19	-30.76
LHF	$W\ m^{-2}$	UWM	59.55	23.18	-24.11	-11.79
$Q_S - Q_{20m}$	$g\ kg^{-1}$	SSM/I	1.72	0.61	-0.60	-0.53
$Q_S - Q_{20m}$	$g\ kg^{-1}$	UWM	0.79	0.26	-0.13	-0.01
U_{20m}	$m\ s^{-1}$	SSM/I	3.29	0.96	-1.00	-1.48
U_{20m}	$m\ s^{-1}$	UWM	3.71	0.59	-0.97	-0.8

FIGURE CAPTIONS

Fig. 1. Annual-mean (a) wind stress, (b) latent heat flux, and (c) sensible heat flux, derived from F8 and F11 SSM/I data during 1988-94. Arrows indicate wind stress directions.

Fig. 2. Same as Fig. 1, except for UWM/COADS during 1990-93.

Fig. 3. Annual-mean (1988-94) (a) 10-m wind speed, and (b) sea-air (10 m) humidity difference, derived from F8 and F11 SSM/I data, and (c) sea-air (2 m) temperature difference of ECMWF.

Fig. 4. Same as Fig. 3, except for UWM/COADS during 1990-93 at a 20-m reference height.

Fig. 5. SSM/I-minus-UWM/COADS differences of (a) wind stress, (b) latent heat flux, and (c) sensible heat flux for 1990-93. Arrows indicate wind stress difference directions.

Fig. 6. SSM/I-minus-UWM/COADS differences of (a) 20-m wind speed, (b) sea-air (20 m) humidity difference, and (c) sea-air (20 m) temperature difference for 1990-93.

Fig. 7. Annual-mean (1990-93) 20-m specific humidity for (a) SSM/I, (b) UWM/COADS, and (c) UWM/COADS-minus-SSM/I difference.

Fig. 8. Seasonal-mean wind stresses for (a) winter, (b) spring, (c) summer, and (d) fall, derived from F8 and F11 SSM/I data during 1988-94. Arrows indicate wind stress directions.

Fig. 9. Same as Fig. 8, except for 10-m wind speeds.

Fig. 10. Same as Fig. 8, except for latent heat fluxes.

Fig. 11. Same as Fig. 8, except for sea-air (10 m) humidity differences.

1988–94 Annual Mean SSMI Fluxes

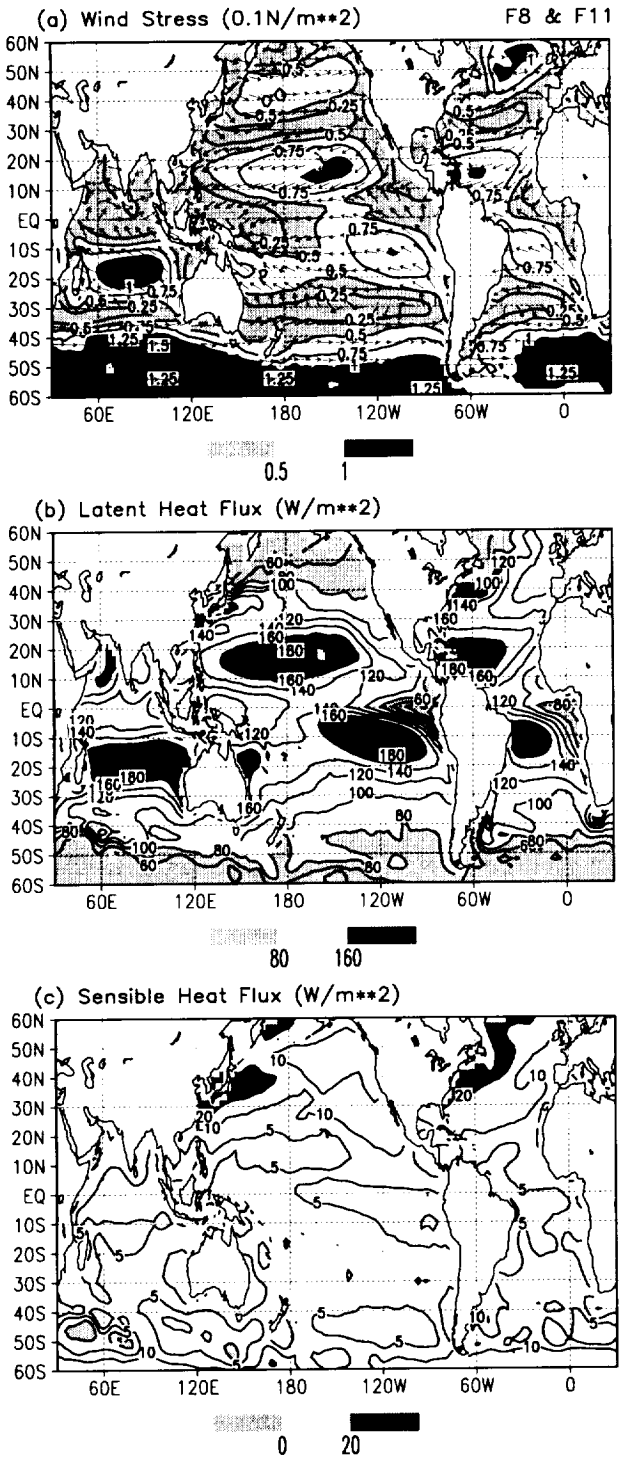

Fig. 1

1990–93 Annual Mean UWM/COADS Fluxes
2x2.5

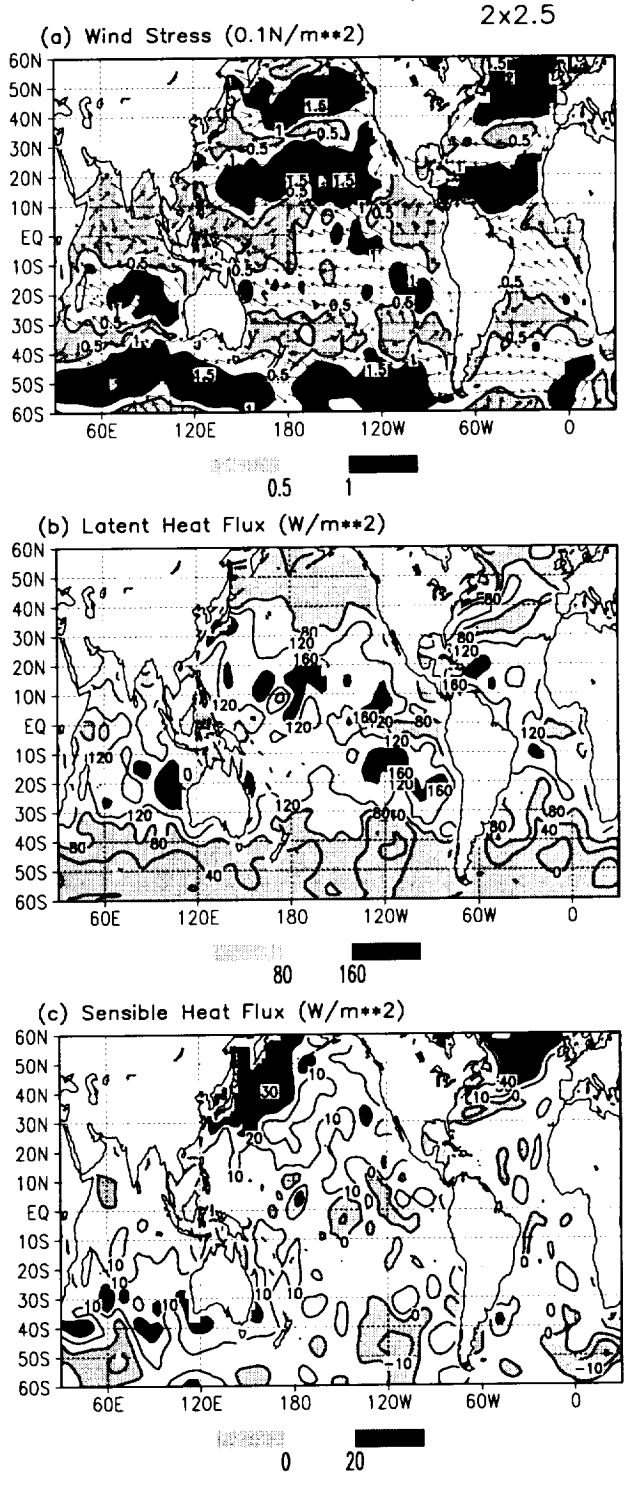

Fig. 2

1988–94 Annual Mean SSMI Parameters

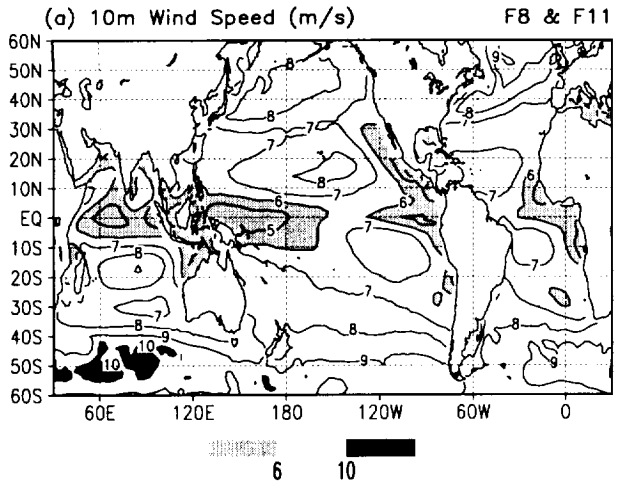

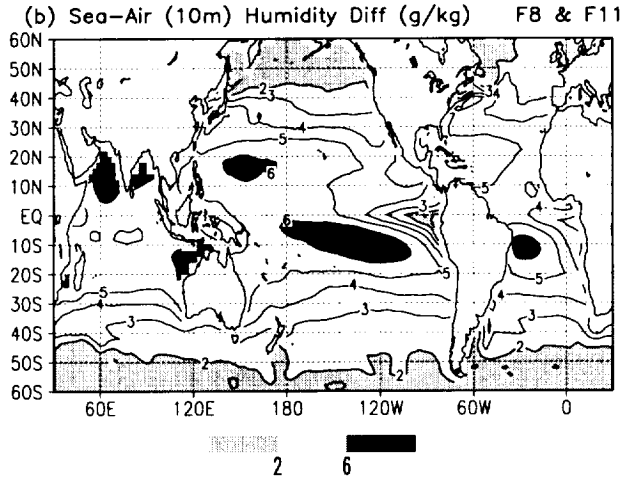

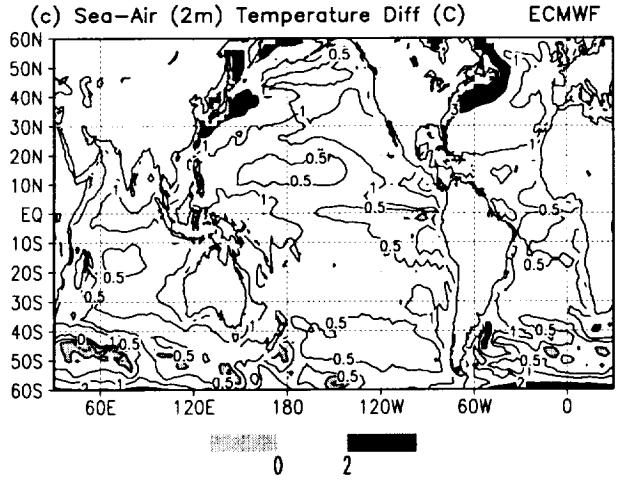

Fig. 3

1990–93 Annual Mean UWM/COADS Parameters

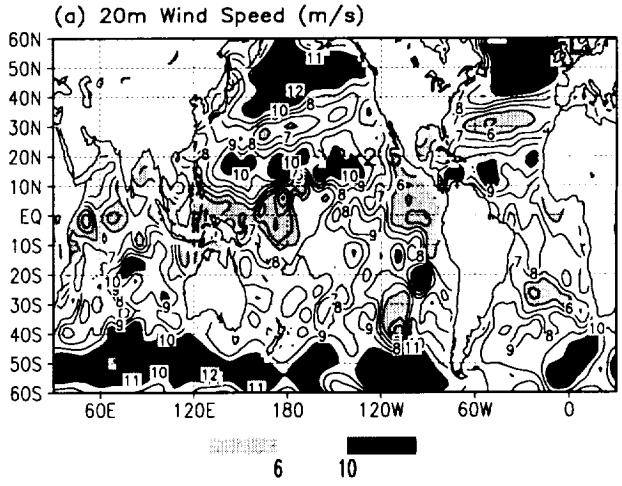

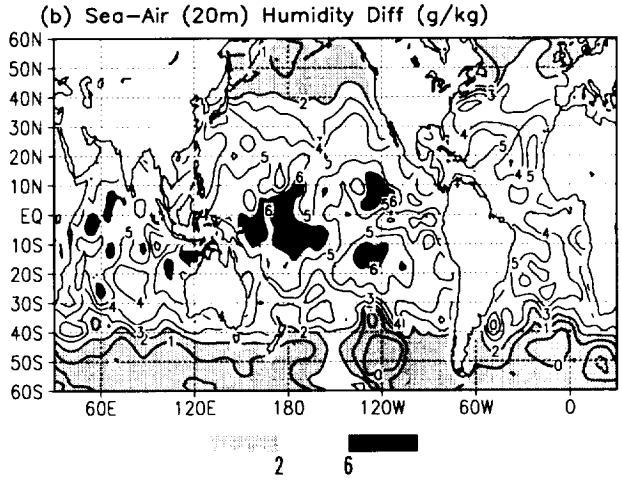

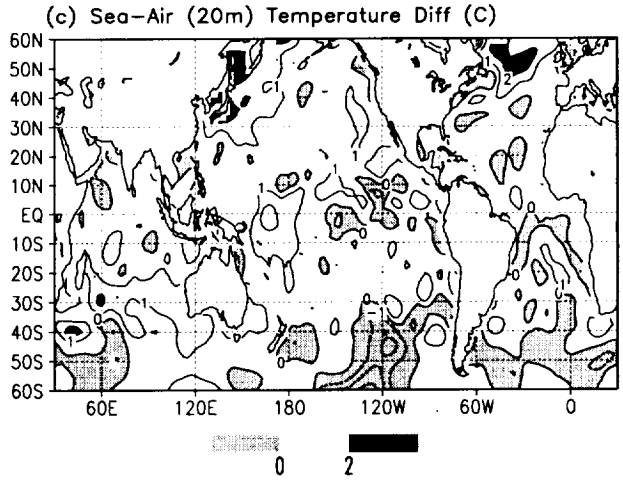

Fig. 4

90–93 Annual Mean SSMI–UWM/COADS Diff

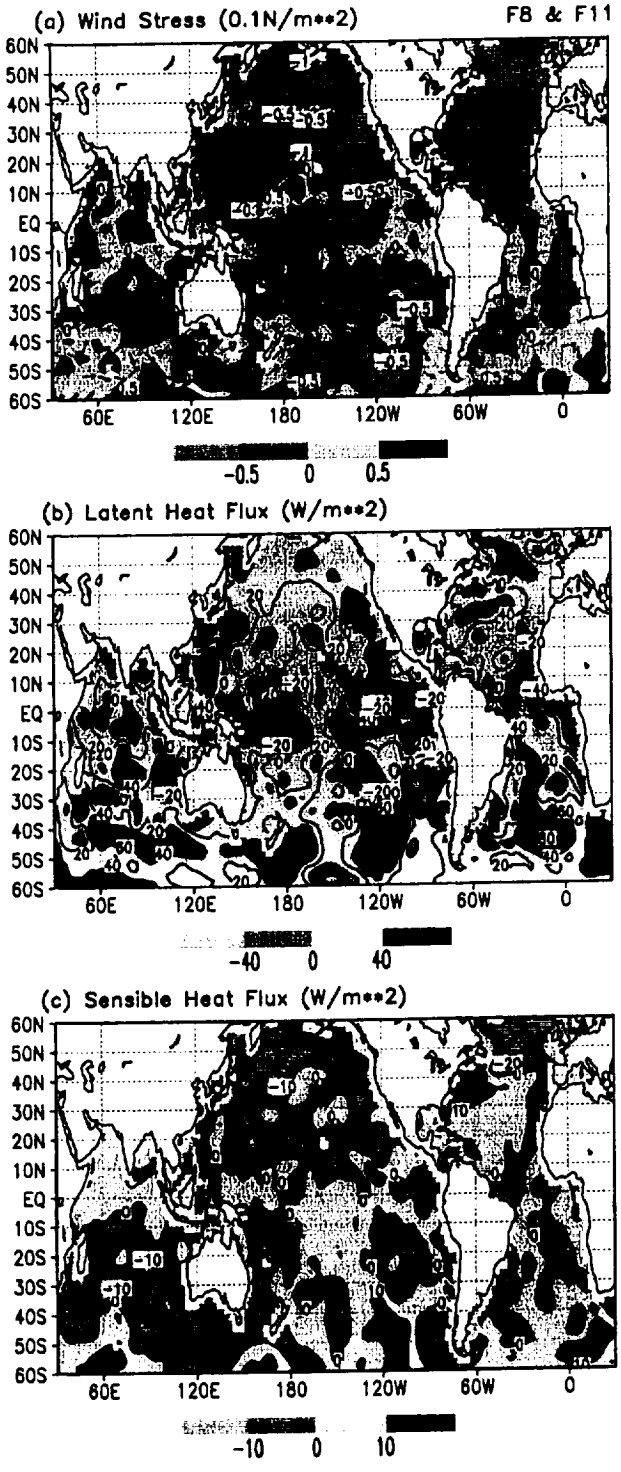

Fig. 5

90–93 Annual Mean SSMI–UWM/COADS Diff

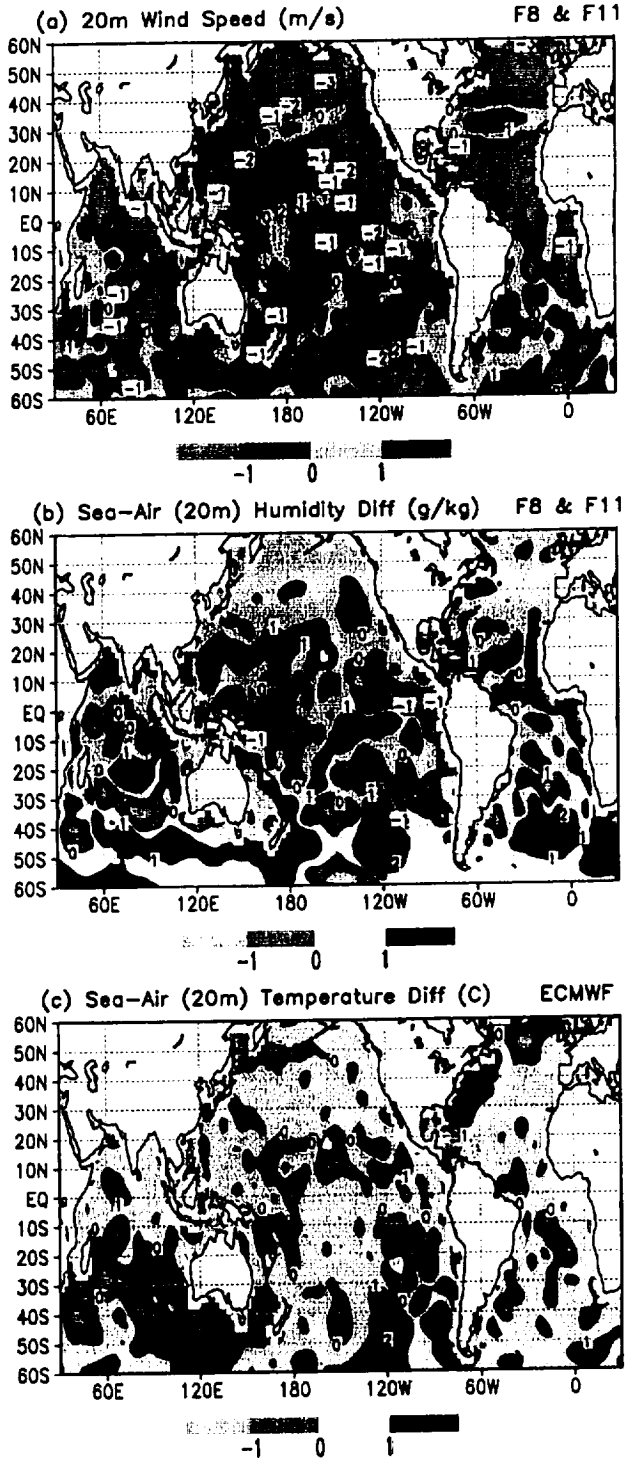

Fig 6

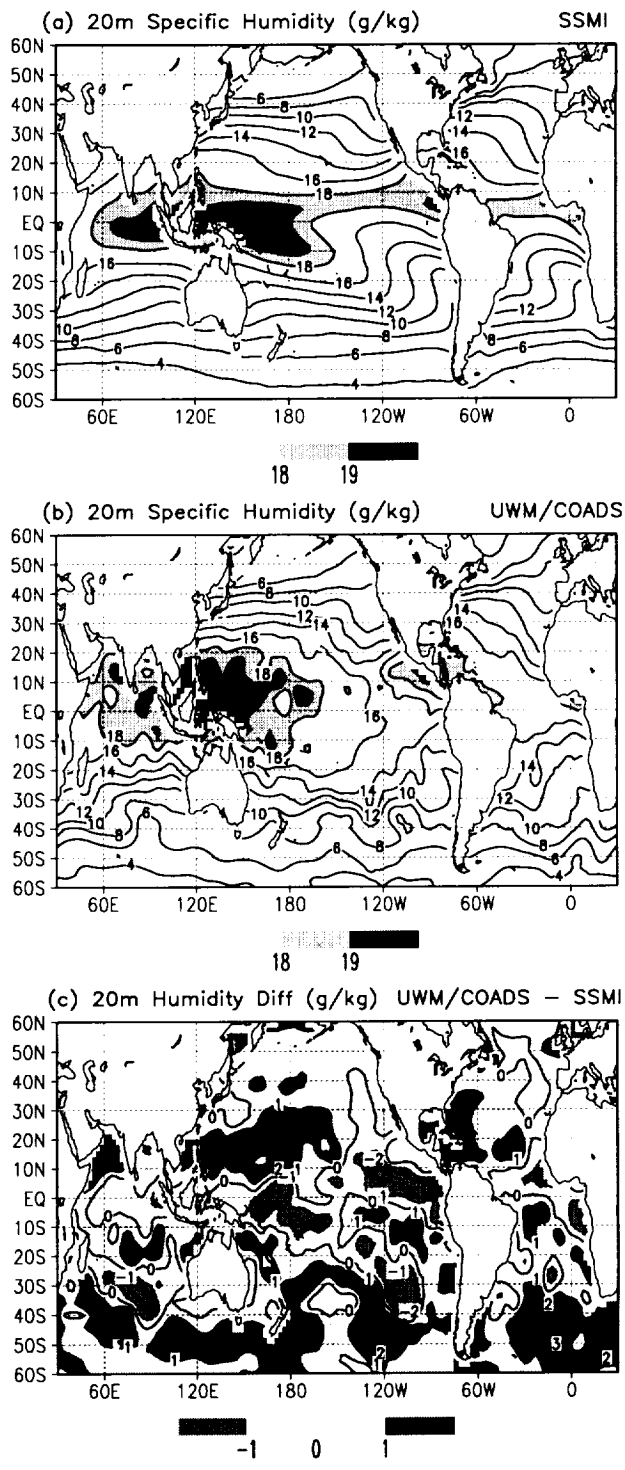
1990–93 Annual Mean Parameters
(a) 20m Specific Humidity (g/kg)
SSMI
(b) 20m Specific Humidity (g/kg)
UWM/COADS
(c) 20m Humidity Diff (g/kg) UWM/COADS – SSMI
60N
50N
40N
30N
20N
10N
EQ
10S
20S
30S
40S
50S
60S
60E
120E
180
120W
60W
0
18
19
-1
0
1

Fig. 7

Fig. 8

Seasonal Mean SSMI Wind Stress (0.1 N/m**2)

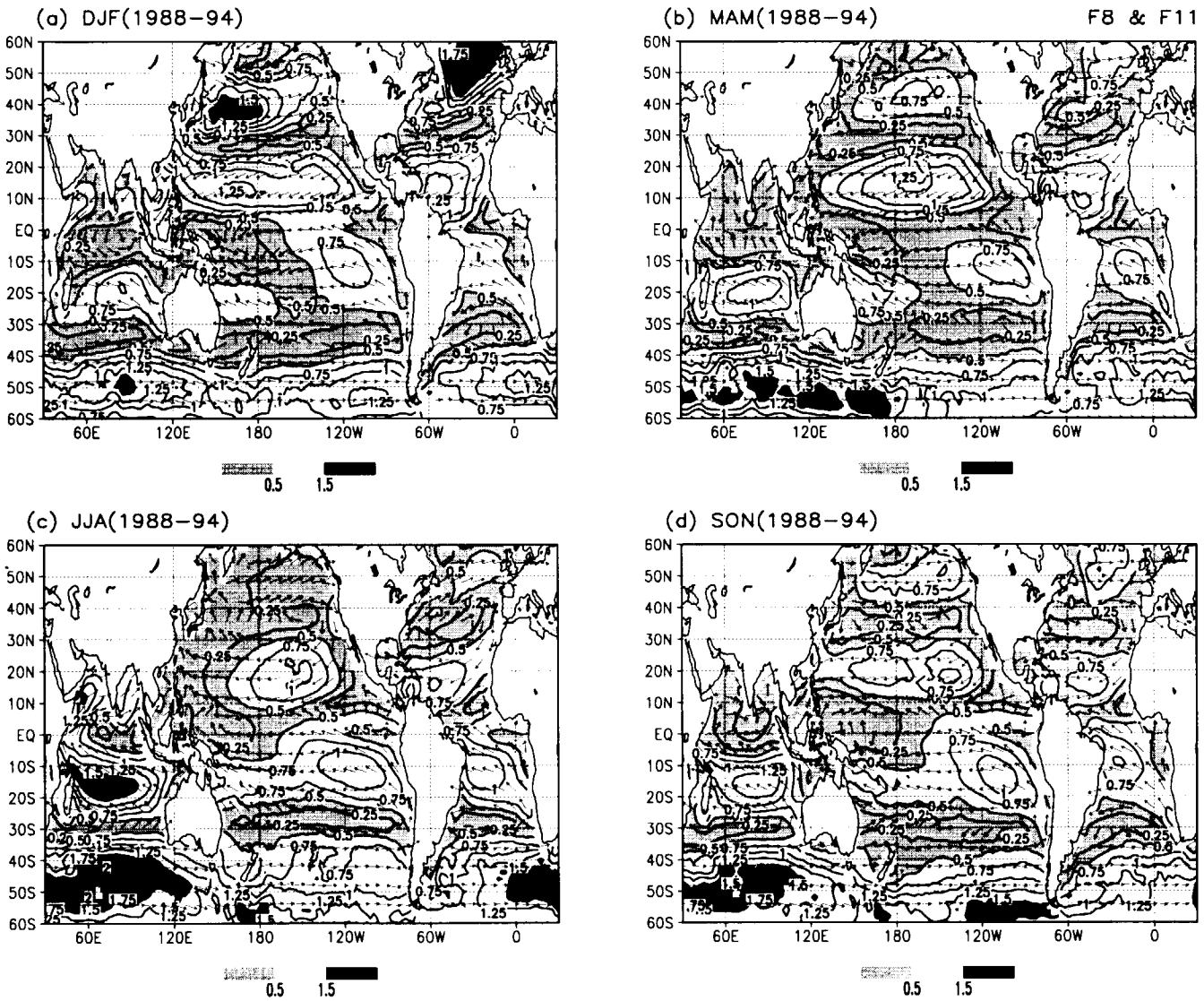

Seasonal Mean SSMI 10m Wind Speed (m/s)

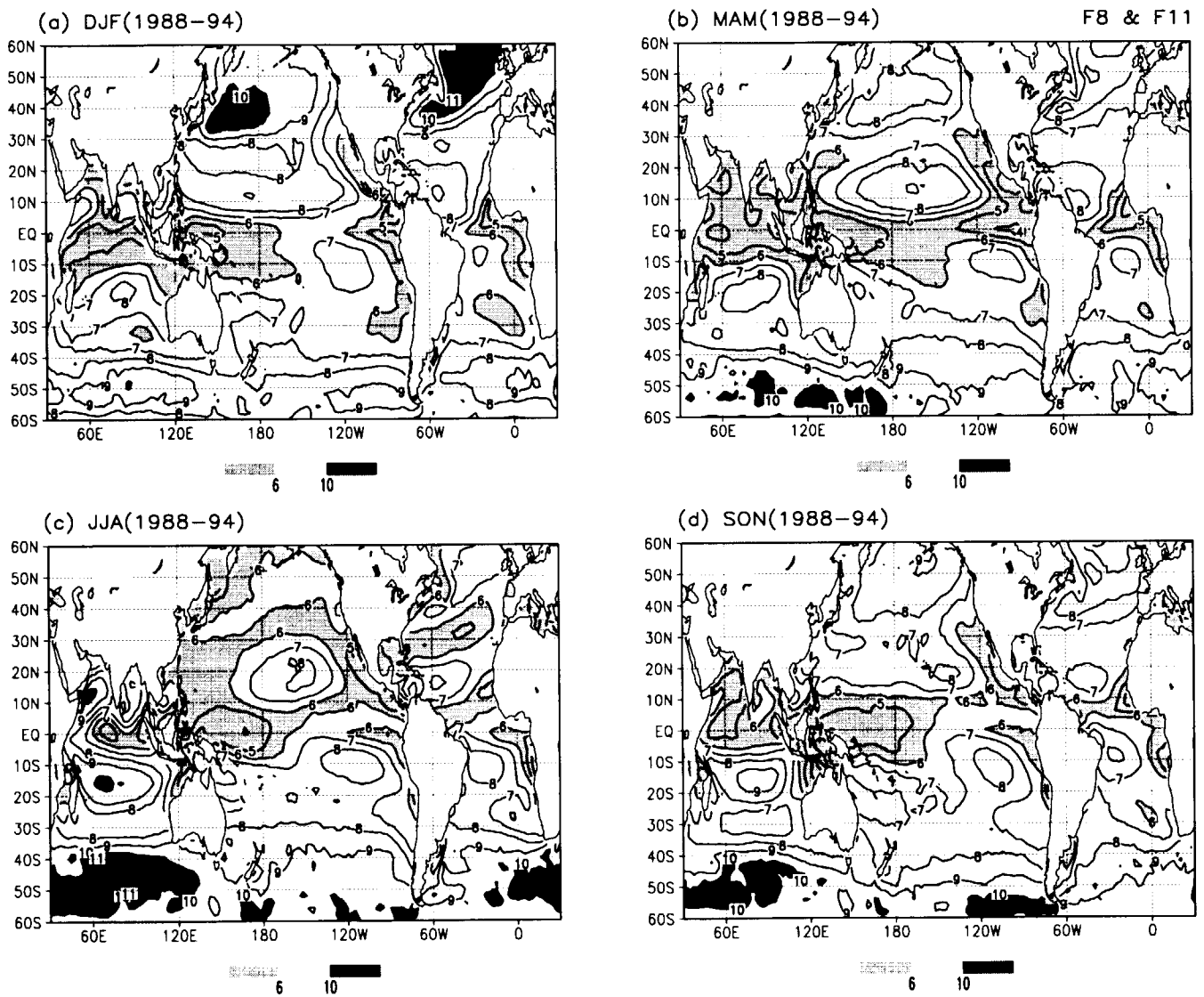

1,9,9

Seasonal Mean SSMI Latent Heat Flux (W/m**2)

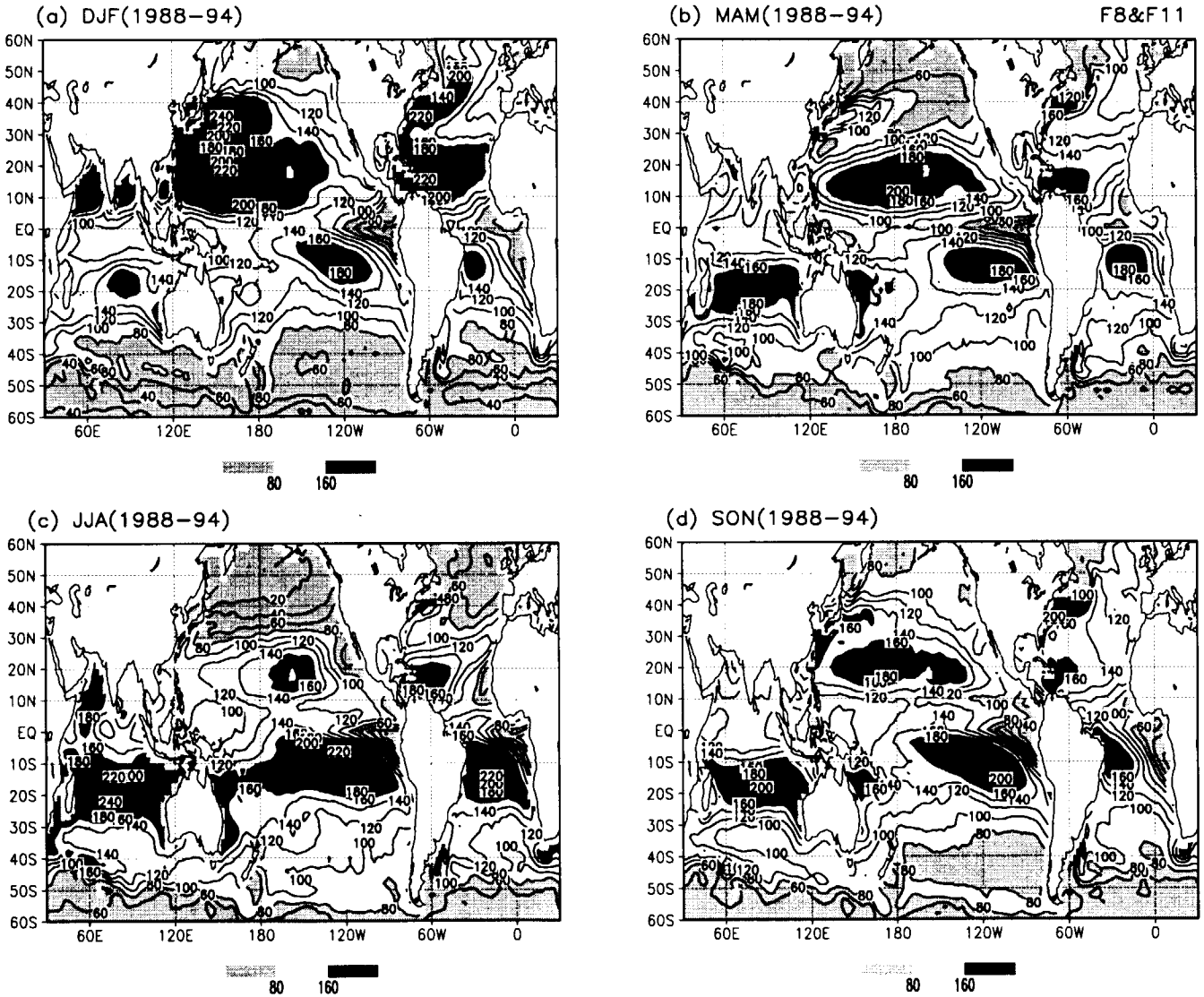

Fig. 12

Fig. 11

Seasonal Mean SSMI Sea–Air (10m) Humidity Diff (g/kg)

(a) DJF(1988–94)

(b) MAM(1988–94) F8 & F11

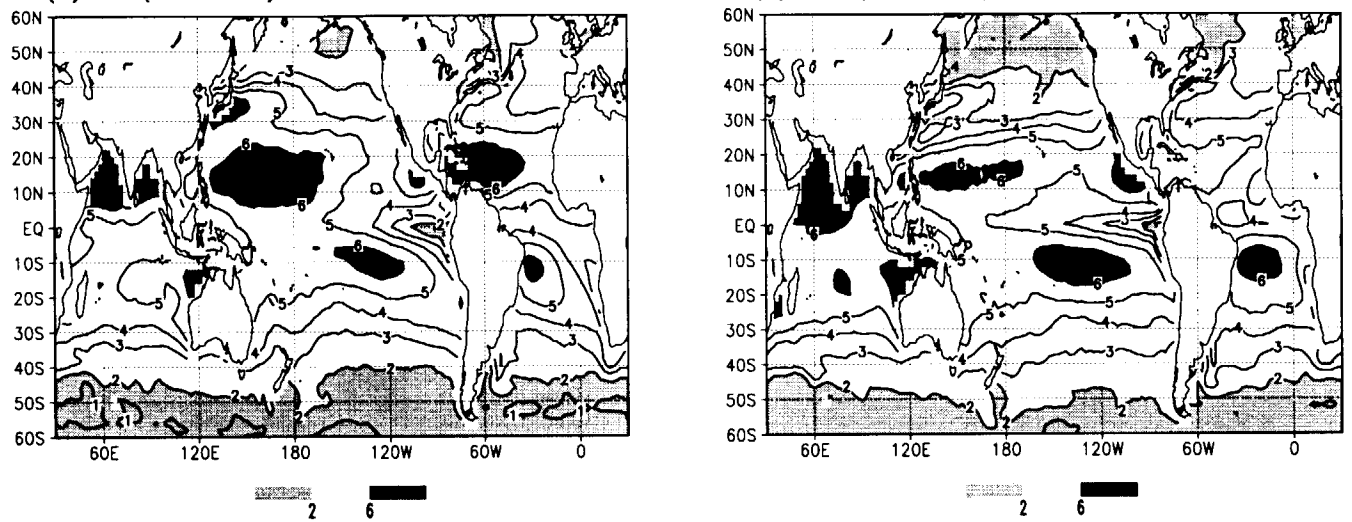

(c) JJA(1988–94)

(d) SON(1988–94)